A complete quantum mechanical study of chlorine photodissociation

A. J. Johnsen, A. B. Alekseyev, G. G. Balint-Kurti, M. Brouard, Alex Brown et al.

Citation: J. Chem. Phys. **136**, 164310 (2012); doi: 10.1063/1.4704829
View online: http://dx.doi.org/10.1063/1.4704829
View Table of Contents: http://jcp.aip.org/resource/1/JCPSA6/v136/i16
Published by the American Institute of Physics.

A complete quantum mechanical study of chlorine photodissociation

A. J. Johnsen,[1] A. B. Alekseyev,[2] G. G. Balint-Kurti,[3] M. Brouard,[1,a)] Alex Brown,[4] R. J. Buenker,[2] E. K. Campbell,[1] and D. B. Kokh[2]
[1]*The Department of Chemistry, University of Oxford, The Physical and Theoretical Chemistry Laboratory, South Parks Road, Oxford OX1 3QZ, United Kingdom*
[2]*Fachbereich C-Mathematik und Naturwissenschaften, Bergische Universität, Gaussstr. 20, D-42119 Wuppertal, Germany*
[3]*Centre for Computational Chemistry, School of Chemistry, University of Bristol, Bristol BS8 1TS, United Kingdom*
[4]*Department of Chemistry, University of Alberta, Edmonton, Alberta T6G 2G2, Canada*

(Received 26 January 2012; accepted 30 March 2012; published online 27 April 2012)

A fully quantum mechanical dynamical calculation on the photodissociation of molecular chlorine is presented. The magnitudes and phases of all the relevant photofragment *T*-matrices have been calculated, making this study the computational equivalent of a "complete experiment," where all the possible parameters defining an experiment have been determined. The results are used to simulate cross-sections and angular momentum polarization information which may be compared with experimental data. The calculations rigorously confirm the currently accepted mechanism for the UV photodissociation of Cl_2, in which the majority of the products exit on the $C\,^1\Pi_{1u}$ state, with non-adiabatic couplings to the $A\,^3\Pi_{1u}$ and several other $\Omega = 1$ states, and a small contribution from the $B\,^3\Pi_{0^+u}$ state present at longer wavelengths. © *2012 American Institute of Physics*. [http://dx.doi.org/10.1063/1.4704829]

I. INTRODUCTION

Molecular chlorine photodissociation has for some time been a benchmark in studies of unimolecular reaction dynamics. Considered to be a vital component in the mechanism of ozone depletion,[1] Cl_2 is one of the ten most produced chemicals in industry.[2] It has also been a testing ground for the development of new techniques,[3–7] providing the basis for several ground-breaking studies on photofragment polarization,[5,8,9] in particular the first paper to link the fully quantum mechanical expressions of Siebbeles *et al.*[10] to ion imaging.[5] Much easier to study experimentally than hydrogen or fluorine, yet still sufficiently simple to be amenable to detailed theoretical studies, Cl_2 photodissociation has been the target of several high level potential energy surface calculations and, crucially, of angular momentum polarization studies over a range of wavelengths throughout its UV absorption spectrum.[8,9,11,12] Angular momentum polarization – the populations of (and coherences between) the magnetic sublevels of the photofragments – gives important information about the shape of the electron cloud in the recoiling atoms, and so provides direct insight into the 'fabric' of the potential energy curves on which the photodissociation takes place.[13] These studies have been complemented by several semi-classical dynamics calculations[14,15] into Cl_2 photodissociation, and together they have resolved important aspects of the fragmentation process.

The need to perform high level quantum dynamics calculations is still pressing, however. The semi-classical calculations employed have often relied on experimentally derived assumptions, or neglected coherence between interfering photodissociation pathways. *Ab initio*, fully quantum mechanical dynamical studies provide another yardstick for the accuracy of these assumptions, hence providing a direct test of how accurately these most subtle and counterintuitive of phenomena can be captured by the theory and on the approximations on which they rely.

This paper presents a new set of fully quantum mechanical results modeling these electronic polarization phenomena. Time dependent wavepacket methods have been employed to extract both partial absorption cross-sections, and angular momentum polarization information at a range of energies encompassing the first absorption band of Cl_2. The methods employed in the calculations are described briefly in Sec. II. The main focus of the present work, given in Sec. III, is the presentation and discussion of the results of these calculations. In the accompanying paper,[16] new experimental data will be presented, and compared in detail with both previous experimental work and the results of the current theory. The implications of the present study for a detailed understanding of chlorine photodissociation are discussed in Sec. IV. The remainder of this introductory section is devoted to a brief description of the notation we employ, and of previous experimental and theoretical work on Cl_2 photodissociation.

A. Notation

The Cl_2 photodissociation processes studied in this paper all correlate to the $Cl(^2P^o) + Cl(^2P^o)$ product channel. Due to spin-orbit coupling, the $Cl(^2P^o)$ atoms can exist in two different *J* states, $Cl(^2P_{3/2})$, and the higher energy $Cl(^2P_{1/2})$, separated by 881 cm^{-1}. Following the notation of Asano and Yabushita,[14] these states will be labelled as $Cl(^2P_{3/2}) \equiv Cl$ and

a)Electronic mail: mark.brouard@chem.ox.ac.uk.

TABLE I. Correspondence between the mixed Hund's case (a)/(c) labels employed here, and their Hund's case (c) equivalents.

Mixed Hund's case (a)/(c) label	Hund's case (c) label
$X\,^1\Sigma_{0g}^+$	$(1)0_g^+$
$A\,^3\Pi_{1u}$	$(1)1_u$
$B\,^3\Pi_{0^+u}$	$(1)0_u^+$
$C\,^1\Pi_{1u}$	$(2)1_u$
$(1)\,^3\Sigma_{1u}^+$	$(3)1_u$
$(1)^3\Delta_{1u}$	$(4)1_u$

$Cl(^2P_{1/2}) \equiv Cl^*$. The $Cl(^2P^o) + Cl(^2P^o)$ asymptote is therefore split into three different exit channels, (Cl + Cl), (Cl + Cl*), and (Cl* + Cl*), with an energy separation between each of 881 cm^{-1}.

The adiabatic states used in the dynamical calculations will be labeled using a mixed Hund's case (a) and (c) notation, again as employed Asano and Yabushita.[14] The correspondence with the alternative Hund's case (c) labels is given in Table I.

B. Previous experimental work

1. Absorption spectrum and dissociation dynamics

The ultraviolet absorption spectrum of molecular chlorine consists of a single broad, bell shaped distribution running from 250 to 450 nm, with a maximum around 335 nm, and arises primarily as a result of excitation to the unbound, repulsive, $C\,^1\Pi_{1u}$ state. A weaker spin-forbidden transition to the $B\,^3\Pi_{0^+u}$ state becomes prevalent in the long wavelength region giving the distribution a slight asymmetry, as illustrated in Fig. 1. Of significance to this absorption band are the two product channels, (Cl + Cl), and (Cl + Cl*), corresponding to the ground and (first) excited state product channels, respectively. The major channel produces ground state chlorine atoms, preferentially dissociating perpendicularly to the direction of the electric field vector of the light. At longer wavelengths the excited state product channel, Cl + Cl*, becomes more dominant, and the transition becomes increasingly parallel in character.

As Cl_2 is a homonuclear diatomic molecule, its electronic states have a definite symmetry (u/g) under parity, and as its ground electronic state is of $^1\Sigma_g^+$ symmetry, only u states will therefore be populated in the excitation step of the dissociation. As a consequence of this, in the absence of Coriolis (electronic-rotational coupling) interactions, only the u electronic states need to be included in the dynamics calculations. The electronic states relevant to the present photodissociation study are derived following the promotion of a single electron between two antibonding orbitals of π_g and σ_u symmetries, respectively. The electronic states derived from the molecular orbitals involved are detailed in the adiabatic correlation diagram shown in Fig. 2. The correlation diagram connects the *molecular* states in both Hunds case (a) and (c) with the separated *atomic* states, and is constructed using the adiabatic correlation rules first described by Mulliken,[17] as also presented in Refs. 6, 8, 18, and 19. As shown in Fig. 2 the $C\,^1\Pi_{1u}$ state

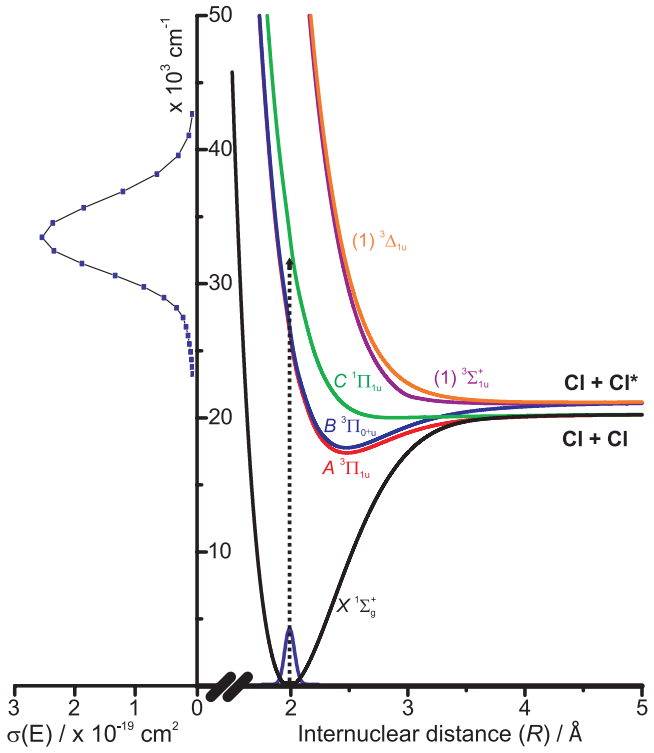

FIG. 1. Adiabatic potential energy curves of Cl_2 (right)[15] important for dissociation in the first absorption band (left).[53] At short wavelengths the $C\,^1\Pi_{1u}$ state (green) dominates with the $B\,^3\Pi_{0^+u}$ state (blue) becoming more important as the wavelength increases.

correlates adiabatically with the ground state product channel, while the $B\,^3\Pi_{0^+u}$ state, important in the enhanced long wavelength portion of the absorption, correlates with the excited state product channel. The adiabatic potential energy curves for the states believed to be important for photodissociation are shown in Fig. 1.

Collectively, the dynamical studies detailed here have led to the currently accepted mechanism for the photodissociation of chlorine within its first absorption band. The dissociation pathway is believed to proceed largely *via* the $C\,^1\Pi_{1_u}$ state, with a strong contribution from the $A\,^3\Pi_{1u}$ state, arising from radial non-adiabatic effects in the asymptotic region of the potentials. As noted above, at longer wavelengths there is also a much weaker excitation to the (spin forbidden) $B\,^3\Pi_{0^+u}$ state, correlating to the excited (Cl + Cl*) channel, which is rendered partially allowed by spin-orbit mixing between the $X\,^1\Sigma_g^+$ and several excited $^3\Sigma_g^-$ states. This channel is of considerable interest, as by the symmetry of the process (a homonuclear ground state molecule coupled to a photon), the two fragments should be symmetrical linear combinations of the two different spin-orbit states. The fact that they are always measured as paired states provides a chemically relevant example of wavefunction collapse.[20] The character of the excited (Cl + Cl*) channel changes with wavelength, becoming more parallel at the red end of the absorption spectrum. The production of excited state Cl* atoms at shorter wavelengths *via* perpendicular excitation is thought to arise from non-adiabatic coupling between the $C\,^1\Pi_u$ state and the excited $(1)^3\Sigma_{1u}^+$ state.[8,14] Dissociation on the highest exit channel leading to two excited chlorine atoms, corresponding to

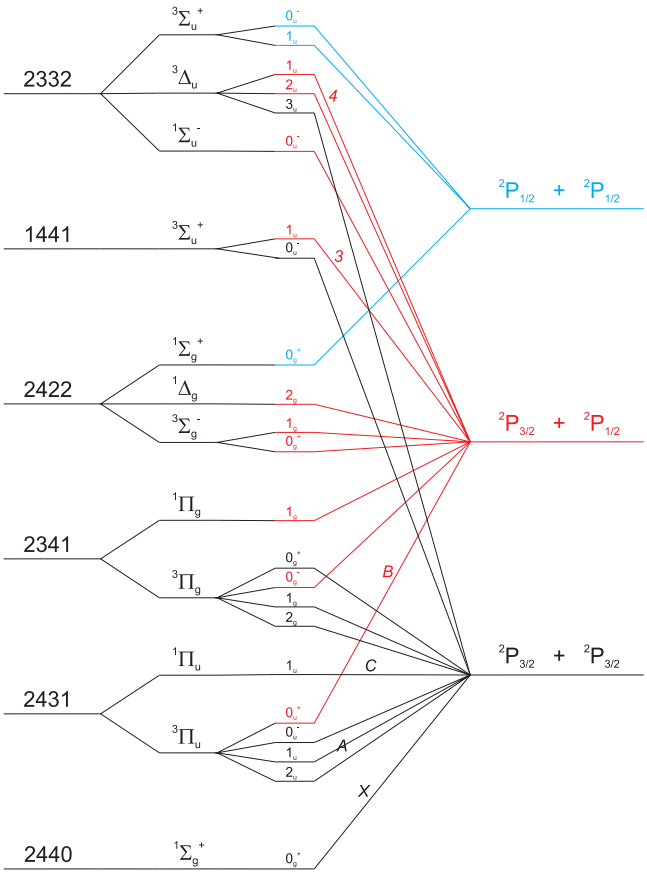

FIG. 2. Adiabatic correlation diagram linking the *atomic* Cl(^2P_J) states (right) with the *molecular* states in Hunds case (c) and (a) (middle), and molecular orbitals (left). The numbers give the occupancy of the $5\sigma_g 2\pi_u 2\pi_g^* 5\sigma_u^*$ molecular orbitals. The five states believed to be important in the photodissociation are also labelled (A, C, B, 3, and 4). Adapted from Refs. 6, 8, 18, and 19.

(Cl* + Cl*), is believed to be negligible in this absorption band.

2. Branching ratios and translational anisotropy

Chlorine photodissociation has been the subject of experimental studies for several decades, using a wide variety of different techniques. Early dynamical studies were performed in the late 1960s by Diesen *et al.*[3] and Busch *et al.*[4] using variants of photofragment translational spectroscopy. Although insensitive to angular momentum polarization effects and the states populated, these studies measured the speed and angular distributions of the fragments, and concluded that the majority of the photofragments were produced in the lowest energy (Cl + Cl) exit channel, in a direction preferentially perpendicular to the electric field vector of the photolysis light. This was assigned to excitation and dissociation only to the C $^1\Pi_{1u}$ state.

Fully state specific determination of the fragments was achieved in 1988 by Li *et al.*,[6] using (3+1) resonantly enhanced multiphoton ionization (REMPI) to detect the atomic products from photodissociation at 325 nm. This confirmed the overwhelming dominance of the (Cl + Cl) channel, and led these researchers to conclude that chlorine photodissociation was 'highly adiabatic' in character; proceeding almost entirely on a single potential energy surface. The (3+1) REMPI scheme employed in Ref. 6 was insufficiently sensitive to detect excited state chlorine atoms. A similar study in 1989 by Matsumi *et al.*[7] used more sensitive (2+1) REMPI, and concluded that the ratio between the ground and excited state Cl atoms at 351 nm was in the ratio of 100:1. A further, more comprehensive study by Matsumi *et al.* in 1992 determined the Cl*/Cl branching ratio over a range of wavelengths between 266 and 500 nm.[18] They concluded that this branching ratio increases at higher wavelength, changing from being almost negligible at 300 nm to ~0.14 at 390 nm. They also found that the spatial anisotropy parameter, β, in the excited state becomes increasingly positive with increasing wavelength. The relative dominance of the ground state exit channel led them to the conclusion that Coriolis coupling in this system is negligible. At short wavelengths, 355 nm, the authors measured a limiting β parameter of −1.0 for the Cl fragments, assigning adiabatic dissociation on the C $^1\Pi_{1u}$ state. On the other hand, the β parameter for the excited Cl* fragment was given as a limiting value of +2.0 at 400 nm, consistent with a pure parallel transition, decreasing to a value of −0.7 at shorter wavelengths of 308 nm, indicating a predominantly perpendicular transition. The parallel component of this channel was assigned to the B $^3\Pi_{0^+u}$ state, with the perpendicular character at shorter wavelengths suggested to arise from non-adiabatic coupling between the C $^1\Pi_{1u}$ and $\Omega = 1$ states correlating with Cl + Cl* at long internuclear distances.

More recently, the first ion imaging study was performed by Samartzis *et al.*[21] using (2+1) and (3+1) REMPI. At 355 nm the authors report β parameters of 1.78 and −0.87 for the Cl* and Cl fragments, respectively, as well as a Cl*/Cl branching ratio ~5 times greater than previously given by Matsumi *et al.*[7,18] Combined, the non-limiting β parameter for the Cl fragments and markedly larger Cl*/Cl branching ratio suggested a greater influence of the B $^3\Pi_{0^+u}$ state on the dissociation dynamics.[21]

3. Atomic alignment measurements

In addition to the above mentioned studies, there have been several investigations into the electronic polarization of both the Cl and Cl* photofragments. The first measurements to probe the atomic alignment in the molecular frame were performed by Wang *et al.*[22] Time-of-flight (TOF) REMPI profiles were recorded using different pump-probe laser polarizations to investigate electronic alignment effects at 355 nm. The authors interpreted their results, utilizing the theoretical description provided by Band *et al.*,[23,24] as showing a preference for the $M_J = \pm 1/2$ sublevels, consistent with adiabatic dissociation on the C $^1\Pi_{1u}$ state.

In 1997 Bracker *et al.* were able to directly link the fully quantum mechanical treatment of atomic polarization effects in the recoil frame[10] with experimentally measurable signals.[25] For the first time a description of the underlying physics of the dissociation that result in atomic polarization effects was provided.[25] Although pre-dating velocity mapping, their ion imaging study used a combination of different

pump-probe laser polarizations and Cl (2+1) REMPI transitions in order to extract the $K = 2$ alignment parameters, rigorously including coherent alignment effects at 355 nm.[5,25] The authors showed that in addition to the incoherent alignment resulting from dissociation on the $C\,^1\Pi_{1u}$ state, a description including a non-adiabatic transition to the $A^3\Pi_{1u}$ state in the long range region of the potentials is required to understand the measured coherent effects.

In 1999 Zare and co-workers[26] performed TOF REMPI experiments to probe the Cl alignment at two wavelengths, 320 nm and 470 nm. Close to the absorption maximum at 320 nm Zare and coworkers found the measured incoherent and coherent alignment to be in agreement with previous work at 355 nm. At the 470 nm tail of the absorption, only incoherent contributions to the alignment were found, with the Cl fragments showing a strong (near limiting) preference for $M_J = \pm 1/2$ and a positive spatial anisotropy, $\beta \sim 2.0$, consistent with adiabatic dissociation on the $B\,^3\Pi_{0^+u}$ state potential. Around the same time Samartzis *et al.* performed a comprehensive ion imaging study, recording ion images of the Cl and Cl* fragments at several dissociation wavelengths from 310–450 nm.[27] The ion images, all recorded with linearly polarized light with the electric vectors of both pump and probe radiation in the plane of the detector, were used to investigate the Cl*/Cl branching ratio and spatial anisotropy parameters for both fragments, in addition to probing the angular momentum alignment effects of the Cl products. For the ground state product channel the angular distributions extracted from the ion images, analyzed using the Abel inversion method, were found to be characterized, within experimental error, by a wavelength independent β_2 component of value -1 with zero contribution from higher order moments. Although the lack of higher order moments in the angular distribution indicates negligible alignment in the laboratory frame, the authors explain that for this particular pump-probe geometry, the same sign and similar magnitude incoherent and coherent alignment in the *molecular* frame can lead to this at first surprising result. The authors also noted that this was consistent with the previously reported values of Bracker *et al.*[5] The distributions for the Cl fragments belonging to the excited state product channel suggested a limiting spatial anisotropy parameter, $\beta = 2.0$, and maximum alignment in the molecular frame, $M_J = \pm 1/2$, for the region 375–450 nm. For this channel the β parameter was shown to decrease with decreasing wavelength below 375 nm, reaching a value of -0.64 at 310 nm. In agreement with the previous work near the absorption peak, a later slice imaging study by Rakitzis and Kitsopoulos,[28] also at 355 nm, showed a preference for $M_J = \pm 1/2$ in the recoil frame for the ground state product channel.

The most recent ion imaging study of Cl alignment was performed by Brouard and co-workers at 308 nm.[12] By recording ion images using several laser pump-probe geometries and (2+1) REMPI transitions, the authors were able to extract the spatial anisotropy parameter, β, and all $K = 2$ alignment terms from their experimental data. The analysis yielded a non-limiting β of -0.9. It was noted that the rotational temperature of the molecular beam had to be in the range 50–100 K to account for the reduction in β on the basis of the electronic transition being purely perpendicular in character. The alignment parameters were found to be in good accord with previous studies at 355 nm,[5] and illustrate the importance of coherence effects even at this short wavelength. Tables II and III provide a summary of the previous laboratory and molecular frame angular momentum alignment measurements.

4. Atomic orientation measurements

In addition to the electronic alignment of the Cl photofragments, two studies have also probed the $K = 1$ orientation of both the Cl and Cl* photofragments. The first such study by Kim *et al.* reported values of the coherent $\mathrm{Im}[a_1^{(1)}(\|, \perp)]$ parameter for the Cl* fragments following dissociation in the range 270–400 nm using linearly polarized light.[9] The $\mathrm{Im}[a_1^{(1)}(\|, \perp)]$ parameter, which was believed to arise following interference between the parallel, $B\,^3\Pi_{0^+u}$ state, and perpendicular, $C\,^1\Pi_{1u}$ state, pathways was shown to oscillate as a function of dissociation wavelength. The authors also reported measurements for the $^{37}Cl^*(^2P_{1/2})$ fragment, which shows a phase shift in the $\mathrm{Im}[a_1^{(1)}(\|, \perp)]$ parameter due to a difference in the de Broglie wavelengths associated with the ^{35}Cl and ^{37}Cl isotopes.[9] The wavelength dependence of the experimental $\mathrm{Im}[a_1^{(1)}(\|, \perp)]$ parameters for the ^{35}Cl and ^{37}Cl isotopes were modeled theoretically, with qualitative agreement between experiment and theory

TABLE II. Laboratory frame alignment parameters reported from previous studies by Brouard and co-workers,[12] Rakitzis *et al.*,[26] Bracker *et al.*,[25] and Rakitzis and Kitsopoulos[28] at 308, 320, and 355 nm, respectively, for the Cl photofragments in the ground state product channel, and from Samartzis *et al.*[27] and Rakitzis *et al.*[26] for the excited state product channel. Errors (1σ) in the final digit(s) are given in parenthesis where appropriate.

	Wavelength (nm)					
Parameter	308 (Ref. 12)	320 (Ref. 26)	355 (Ref. 25)	355 (Ref. 28)	375–450 (Ref. 27)	470 (Ref. 26)
β	−0.88(3)	−1.0	−1.0	−1.0	∼2.0	∼2.0
s_2	−0.12(2)	−0.10(2)	−0.074(9)	−0.10(2)	−0.16	−0.14(4)
α_2	−0.06(1)	−0.05(1)	−0.032(3)	−0.05(1)	0.16	0.14(4)
γ_2	−0.05(1)	...	0.001(16)	...	...	...
η_2	0.16(4)	0.16(3)	0.075(20)	0.15(5)	...	...
$\langle A_{20}\rangle$	−0.10(6)	−0.10(7)	−0.09(8)	−0.08(10)	−0.32	−0.28(8)

TABLE III. Molecular frame alignment parameters reported from previous studies by Brouard and co-workers,[12] Rakitzis *et al.*,[26] Bracker *et al.*,[25] Rakitzis and Kitsopoulos,[28] and Samartzis *et al.*[27] $a_0^{(2)}(\perp)$ and $a_2^{(2)}(\perp)$ data are shown for the Cl fragments in the ground state product channel (top) while $a_0^{(2)}(\parallel)$ data are shown for the excited state product channel (bottom). Errors (1σ) in the final digit(s) are given in parenthesis where appropriate.

	Wavelength (nm)					
Parameter	308 (Ref. 12)	320 (Ref. 26)	355 (Ref. 25)	355 (Ref. 28)	375–450 (Ref. 27)	470 (Ref. 26)
β	−0.88(3)	−1.0	−1.0	−1.00(3)	∼2.0	∼2.0
$a_0^{(2)}(\perp)$	−0.62(9)	−0.50(10)	−0.35(4)	−0.50(10)	...	...
$a_2^{(2)}(\perp)$	−0.26(7)	−0.32(6)	−0.15(4)	−0.30(10)	...	...
$a_0^{(2)}(\parallel)$	...	...	...	...	∼−0.8	−0.70(20)

observed. In a separate study Alexander *et al.* used circularly polarized photolysis light to measure the incoherent orientation, $a_0^{(1)}(\perp)$, for the Cl and Cl* fragments following dissociation at 310 and 330 nm.[8] The authors found that for the ground state product channel the measured $a_0^{(1)}(\perp)$ parameters were consistent with dissociation on the $C\,^1\Pi_{1u}$ state potential with a contribution arising from the $A\,^3\Pi_{1u}$ state due to a non-adiabatic transition between the two. A mechanism based on a small fraction of the excited $C\,^1\Pi_{1u}$ state molecules making a non-adiabatic transition to the $(1)^3\Sigma_{1u}^+$ state was necessary to explain the Cl* orientation. It was proposed that of the 88% of Cl* fragments which arise from excitation to the C state, ∼67 % of Cl* atoms dissociate on the $(1)^3\Sigma_{1u}^+$ surface, while ∼21 % undergo a further non-adiabatic transition to the $(1)^3\Delta_{1u}$ state along the dissociation coordinate.[8] A summary of the previously measured laboratory and molecular frame $K = 1$ orientation moments is provided in Tables IV and V.

C. Previous theoretical studies

As would be expected for a molecule of its importance and simplicity, there have been several different studies of Cl_2 photodissociation, spanning three decades. The first set of potential energy curves was calculated by Peyerimhoff and Buenker,[29] using a multireference configuration interaction method. The results accurately described both the qualitative shape of the potential curves and the energy ordering of the states, although neglected the spin-orbit coupling interaction.

More recently, in the last ten years there have been several high-level studies determining the Cl_2 potential energy curves. In 2001 Asano and Yabushita[14] performed a calculation using the 'contracted SOCI' method, which gave a full set of adiabatic potentials for the $\Omega = 0$ and $\Omega = 1$ states, including the spin-orbit interaction. This was used in a semi-classical study of the photodissociation, with the non-adiabatic couplings calculated using the Rosen-Zener-Demkov approximation. Using a method based on the Young's double slit model,[30] they were able to approximately reproduce both the magnitude and phase of the oscillatory structure on the photolysis wavelength-dependent orientation polarization parameter, $\mathrm{Im}[a_1^1(\parallel, \perp)]$, measured in the work of Zare and co-workers.[9] This effect was attributed to interference between the $B\,^3\Pi_{0^+u}$ and $(1)^3\Sigma_{1u}^+$ states, where the latter was populated by radial non-adiabatic coupling to the $C\,^1\Pi_{1u}$ state.

In a pair of papers in 2001 and 2004, further sets of potentials due to Kokh *et al.* were presented,[31,32] using relativistic core potentials and the generalized Davidson correction to produce sets of adiabatic potentials including the spin-orbit interaction. The first paper concentrated on the higher level ion-pair states (which dissociate to Cl^+ and Cl^-),[31] whilst the second paper dealt with the lower lying valence states and performed the calculations to a higher level of accuracy.[32] To achieve this goal, the atomic basis set in Ref. 32 was enlarged to include additional polarization and diffuse functions and the configuration interaction (CI) reference sets were adapted for a more accurate description of the lower valence states. The CI selection threshold was significantly lowered to $T = 0.02\ \mu E_h$, so that the dimensions of the CI matrices to be diagonalized explicitly increased by a factor of 3–4. In addition, to attain better accuracy for the transition moments, the CI calculations were performed using an even smaller CI

TABLE IV. Laboratory frame orientation parameters reported from previous studies by Kim *et al.*[9] and Alexander *et al.*[8] Note that the authors used the values of the spatial anisotropy, β, from the work of Samartzis *et al.*[27] to calculate their orientation moments. Errors (1σ) in the final digit(s) are given in parenthesis where appropriate.

	Cl		Cl*	
Parameter	318 (Ref. 8)	330 (Ref. 8)	310 (Refs. 8 and 9)	330 (Refs. 8 and 9)
β	−1.0	−1.0	−0.64	0.24
α_1	0.07(1)	0.12(1)	−0.11	−0.08(5)
γ_1'	...	...	−0.15	−0.032(5)

TABLE V. Molecular frame orientation parameters reported from previous studies by Kim *et al.*[9] and Alexander *et al.*[8] Note that the authors used the values of the spatial anisotropy, β, from the work of Samaratzis *et al.*[27] to calculate their orientation moments. Errors (1σ) in the final digit(s) are given in parenthesis where appropriate.

	Cl		Cl*	
Parameter	310 (Ref. 8)	330 (Ref. 8)	310 (Refs. 8 and 9)	330 (Refs. 8 and 9)
β	−1.0	−1.0	−0.64	0.24
$a_0^{(1)}(\perp)$	0.13(2)	0.23(1)	−0.24(1)	−0.26(17)
$\mathrm{Im}[a_1^{(1)}(\parallel, \perp)]$	...	...	∼0.10	0.032(5)

configuration selection threshold of $T = 0.005\ \mu E_h$, and the convergence of the C–X and B–X transitions moments with respect to the T value has been analyzed. Altogether, these changes have allowed the authors to quantitatively reproduce the experimental absorption spectrum, although non-adiabatic couplings were neglected in this work. Due to the method with which they were calculated, they can be easily separated into a diabatic set and a set of non-adiabatic couplings (in this case the spin-orbit interaction). This means they can be adapted fairly easily to deal with non-adiabatic effects, and hence it is these potentials which are employed in the dynamical studies presented in this paper. They are described in greater detail in Sec. II A.

Finally, in 2008 a set of all 23 states corresponding to the production of two $Cl(^2P)$ atoms were calculated, using a complete open shell configuration interaction approach.[2] Although calculated in a way that was unsuitable for the present quantum mechanical (QM) dynamical study, agreement in the spectroscopic quantities calculated for these potentials and the ones of Kokh *et al.* presented in Ref. 32 is extremely good.

In recent years, several photodissociation dynamics studies have also been performed for this system, to differing levels of approximation. In 2003 Asano and Yabushita[15] performed semi-classical calculations using their own set of potentials, and compared them to equivalent calculations for the photodissociation of Br_2. It was found that the chlorine photodissociation pathway exhibited considerably stronger non-adiabatic effects than that of Br_2, which dissociates largely adiabatically. This would be the expected trend for a system with a smaller mass and a weaker spin-orbit coupling interaction.

Previous QM wavepacket dynamical calculations by Balint-Kurti and coworkers[33–35] on the photodissociation of the hydrogen halides are also worthy of special note. Although on different systems to the one chosen for the present study, the methodology adopted was very similar to that employed here. These studies were used to extract the polarization parameters for photodissociation of the hydrogen halides over a range of photon energies, and were in good agreement with available experimental data. The main issue with these systems, however, is that they absorb mostly in the vacuum ultraviolet, beyond the current reach of typical dye laser systems. This makes obtaining experimental polarization parameters across the absorption spectrum challenging, and hence these systems, unlike molecular chlorine, have relatively few data points with which to compare the calculated results.

II. METHOD

A. Potentials

As mentioned already, the potential energy curves used in the calculations were those of Kokh *et al.*,[32] and consisted of a set of *ab initio* curves for the lowest 12 states of Cl_2, correlating to the $Cl(^2P) + Cl(^2P)$ exit channels, and a single ion pair state.[31] The calculations were performed using the multireference singles and doubles configuration interaction method,[36,37] combined with relativistic effective core potentials to account for the non-valence electrons in the atom.[38,39]

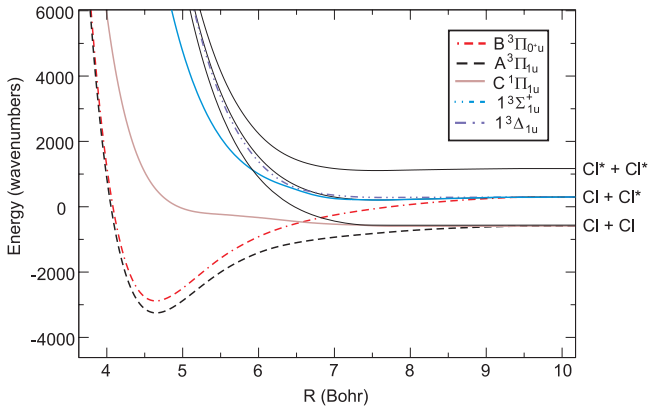

FIG. 3. Diagram of the excited potential energy curves believed to be important in the photodissociation of Cl_2.

These states were then coupled by a set of spin-orbit coupling interaction matrix elements, calculated using the same method. Diagonalization of the resulting matrix leads to a set of potentials with the correct asymptotic atomic energies, and these were used as the fully adiabatic states in our calculations. A more detailed view of these adiabatic potential energy curves is given in Fig. 3.

As discussed by Balint-Kurti and co-workers, the potential energy curves calculated without spin-orbit coupling form an appropriate diabatic basis for this system,[33,34] and were used to propagate the nuclear kinetic energy portion of the Hamiltonian. As the *ab initio* electronic structure calculations required an Abelian point group,[40] these calculations were performed in D_{2h} symmetry. In the D_{2h} point group the $\Omega = 1$ and $\Omega = 3$ states occur within the same irreducible representation and are therefore not distinguished by symmetry. This leads to difficulties in assigning the correct energies to molecular quantum states when their energies cross. Although this had no influence on the results of the dynamics calculations, it had the consequence that the identity of the long range potentials are liable to change multiple times at large nuclear distance, and so the identity of the final states had to be determined by careful inspection of the potential curves.

The transition dipole moments were initially calculated in the diabatic representation, and then diagonalized to take into account spin-orbit couplings, *via* the expression

$$\mu^A_{ji,q}(R) = \sum_{k,l} c_{jk,u}(R)\mu^D_{kl,q}(R)c^*_{il,g}(R)\,. \qquad (1)$$

This required that the diabatic to adiabatic transformation matrices for both the gerade ($c_{il,g}(R)$) and ungerade ($c_{jk,u}(R)$) states were determined. In the diabatic representation, only the fully allowed $^1\Pi_u \leftarrow {}^1\Sigma^+_g$ transition has a non-zero cross-section. The equivalent $C\,^1\Pi_{1u} \leftarrow X\,^1\Sigma^+_{0g}$ transition remains dominant in the adiabatic representation, but weak spin-orbit mixing of the $^1\Sigma^+_g(X)$ and $^3\Pi_g$ states also allows a weak transition to the $^3\Pi_{0^+u}$ state.

Although the potentials were of very high quality (with a configuration selection threshold of $0.02\,\mu E_H$), they still proved insufficiently smooth for the dynamics calculations, and functional fits were required. The fitting was performed using a genetic algorithm, to ensure a full sampling of the

fitting space. Two different functions were used to fit the potentials employed in the dynamics calculations:

- States of an obviously repulsive character were fit using an inverse power series expansion of the form: $V(R) = \sum_n a_n/R^n$, where n ran from 1 to 40. The a_n coefficients were allowed to take positive or negative values.
- The inverse power series was found to converge extremely slowly in the case of states with bound character, and lead to unrealistic artifacts in the long range part of the potential. They were therefore instead fitted to an extended Rydberg potential:[41] $V(R') = -D_e\, e^{-a_1 R'}(\sum_n a_n R'^n)$, in which $R' = R - R_e$, R_e, and D_e are the position and depth of the potential minimum, respectively, and the sum contains polynomial terms up to $n = 8$.

The error in the fits was in all cases less than 0.1%. In the fitting process, the energy gap between the initial and excited states in the Franck-Condon region was found to have shifted by ~1300 cm^{-1}. A uniform shift in energy was therefore applied to the entire $X\,^1\Sigma_g^+$ potential surface, to ensure that the *ab initio* values for the excitation energy were preserved in the dynamical calculations.

The transition dipole moments and spin-orbit coupling matrix were smoother than the potentials, and so could be adapted for the dynamical calculation with a spline interpolation. As described in Sec. III C, dynamical calculations were performed using both R-dependent *ab initio* transition dipole moments, or with constant (R-independent) values in the adiabatic representation.[32] The R-dependent adiabatic transition dipole moments employed are shown in Fig. 4. The various spin-orbit couplings to the $C\,^1\Pi_{1u}$ state are shown in Fig. 5. The initial vibrational wavefunction was calculated using the Fourier Grid Hamiltonian method[42] in the fully adiabatic representation, as this allowed the excitation of the $B\,^3\Pi_{0u}^+$ state to be included as precisely as possible.

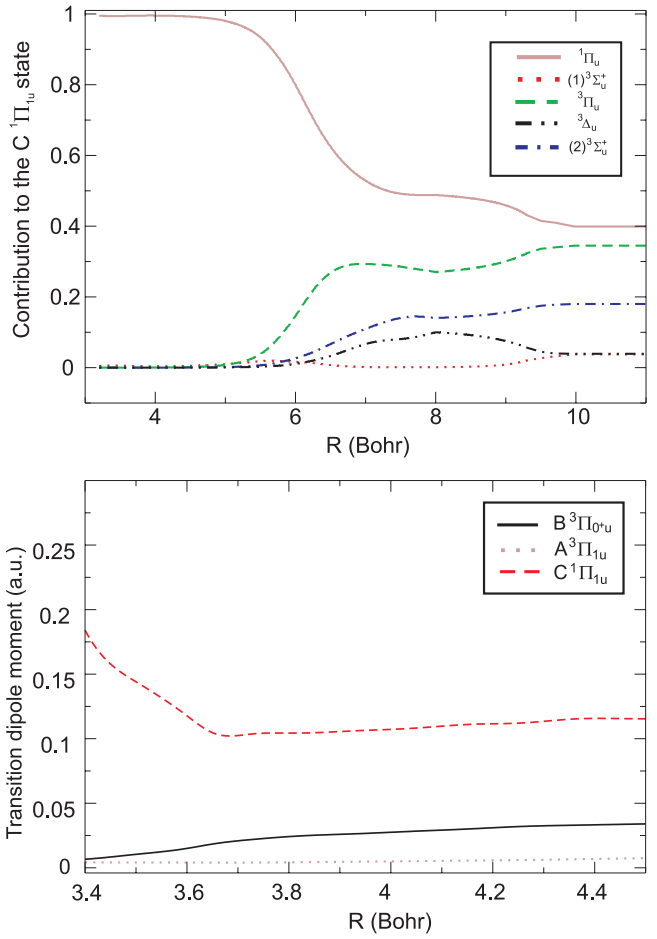

FIG. 4. Top panel: $|c_{jk,u}(R)|^2$ parameters, where j corresponds to the $C\,^1\Pi_{1u}$ state. These quantities correspond to the relative contributions of the different diabatic states to $C\,^1\Pi_{1u}$. When the internuclear separation R is low, the $C\,^1\Pi_{1u}$ state has an almost one-to-one correspondence with the $C\,^1\Pi_{1u}$ state, but at larger R considerable spin-orbit mixing of the diabatic states occurs. Bottom panel: R dependence of the adiabatic transition dipole moments for the bright states of Cl_2 in the Franck–Condon region.

B. Dynamics

The photodissociation calculations were performed using an adapted version of the wavepacket code of Brown and Balint-Kurti, developed for analysis of the photodissociation of the hydrogen halides.[33–35] The initial wavepacket was generated by projecting the ground state wavefunction multiplied by the transition dipole moment onto the excited potentials, and then propagating quantum mechanically until the wavepacket had entirely left the interaction region, and been completely absorbed by the imaginary potential at the end of the grid. In order to ensure complete convergence of the calculations, the propagation of the initial wavepacket was performed using two distinct numerical algorithms: the symmetric split operator[43] and Chebychev polynomial[44] methods. Using the parameters given in Table VI, the partial cross-sections calculated using these methods were found to be in good agreement with each other, deviating by less than 1%.

Non-adiabatic effects were taken into account by transforming the wavepackets to the diabatic representation for the kinetic energy part of the propagation, which allowed flux to flow between the different adiabatic potentials. The wavepacket was sampled at a large value of the scattering coordinate (R_∞) and stored at each time-step, and then Fourier transformed to obtain the photofragment T-matrix elements, using the relationship[33,45]

$$T_{ji}(E) = i\,\frac{1}{2\pi}\left(\frac{h^2 k_j}{2\pi\mu}\right)^{1/2} e^{-ik_j R_\infty}\int_0^\infty dt\; e^{iEt/\hbar}\chi_j(R_\infty, t), \tag{2}$$

where $\chi_j(R_\infty, t)$ is the wavepacket at large separations on the jth potential curve, k_j is the associated scattering wavevector, and μ is the reduced mass of the scattered products. Combinations of the resulting T-matrix elements can be used to determine absorption cross-sections and angular momentum polarization parameters.[10,46] This is achieved *via* the creation of a series of dynamical parameters $f_K(q, q')$, defined by[10,46]

$$f_K(q,q') = \sum (-1)^{K+j_A+\Omega'_A}\begin{pmatrix} j_A & j_A & K \\ -\Omega_A & \Omega'_A & q-q' \end{pmatrix}\left(\mathcal{T}^{n,\Omega}_{J_a J_b \Omega_a \Omega_b}\right)^* \times \mathcal{T}^{n',\Omega'}_{J_a J_b \Omega'_a \Omega_b} T^{(q)*}_{ni}(\Omega, \Omega_i) T^{(q')}_{n'i}(\Omega', \Omega_i), \tag{3}$$

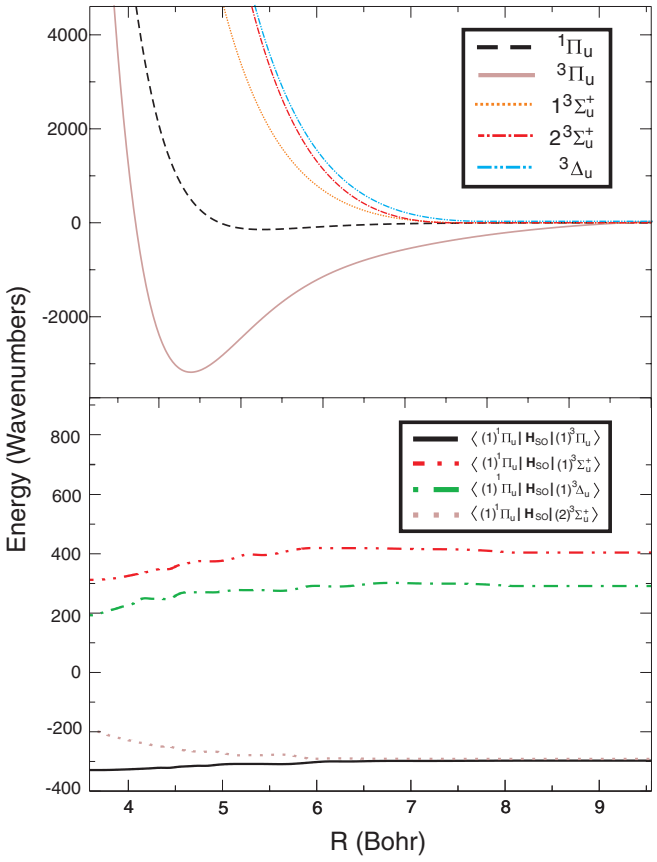

FIG. 5. Top panel: Diabatic potentials for the electronically excited states used in the photodissociation dynamics calculation. The diabatic states are defined by neglecting the spin-orbit couplings. Bottom panel: R-dependence for the spin-orbit couplings to the $C^1\Pi_u$ state.

where q and q' refer to the spherical components of the dipole moment vector (taking the values of $+1$, 0 or -1), and the $\mathcal{T}$ components are the overlap between the atomic fragments and the long range molecular states. The $f_K(q, q')$ can then be related to the experimentally measurable parameters. A comprehensive list of these relationships is provided in the review by Suits and Vasyutinskii,[46] a shortened version for $K \leq 2$ of which is given in Table VII.

Coriolis couplings were ignored in this study, meaning that states of different Ω were decoupled. The effect of Coriolis coupling on molecular chlorine photodissociation has been discussed in several previous papers and is considered to be quite small.[14,15] The polarization parameters were therefore calculated assuming the axial recoil approximation. Parent molecular rotation (treated quasi-classically) and its potential effect on experimental observables, is discussed further in Sec. III D 7.

TABLE VI. Parameters used in the propagation algorithms.

Parameter	Value
Total propagation time (fs)	786
Time-step (fs)	0.024
Number of grid points	2048
Grid spacing (bohr)	0.007
Grid range (bohr)	3.2–18.5
Analysis distance (bohr)	15.0
Start of damping potential (bohr)	15.5
Damping parameter (E_H)	0.059
Number of Chebychev polynomials (Chebychev propagation only)	17

TABLE VII. Definitions of the molecular frame polarization parameters[26,48] in terms of expressions for the dynamical functions, $f_K(q, q')$,[10] and expressions for the laboratory frame polarization parameters of Picheyev *et al.*[46,51] The $V_K(J)$ are J-dependent normalization factors, defined elsewhere.[35,58] Adapted from a more extensive table presented in Ref. 46. Note that $V_2(J) = 2.795$ for $J = 1.5$.

Molecular frame	Dynamical function	Laboratory frame
$a_0^{(1)}(\perp)$	$\frac{f_1(1,1)}{f_0(1,1)}$	$\frac{6}{2-\beta}\alpha_1$
$\mathrm{Re}[a_1^{(1)}(\parallel, \perp)]$	$\frac{\mathrm{Re}[f_1(1,0)]}{[2f_0(1,1)+f_0(0,0)]^{1/2}}$	$\frac{3}{2[(2-\beta)(1+\beta)]^{1/2}}\gamma_1$
$\mathrm{Im}[a_1^{(1)}(\parallel, \perp)]$	$\frac{\mathrm{Im}[f_1(1,0)]}{[2f_0(1,1)+f_0(0,0)]^{1/2}}$	$\frac{-3}{2[(2-\beta)(1+\beta)]^{1/2}}\gamma_1'$
$a_0^{(2)}(\perp)$	$\frac{5}{V_2}\frac{f_2(1,1)}{f_0(1,1)}$	$\frac{10}{2-\beta}(\alpha_2 + s_2)$
$a_0^{(2)}(\parallel)$	$\frac{5}{V_2}\frac{f_2(0,0)}{f_0(0,0)}$	$\frac{5}{1+\beta}(s_2 - 2\alpha_2)$
$\mathrm{Re}[a_1^{(2)}(\parallel, \perp)]$	$\frac{-5}{V_2}\frac{\mathrm{Re}[f_2(1,0)]}{[2f_0(1,1)+f_0(0,0)]^{1/2}}$	$\frac{-5\sqrt{3}}{2[(2-\beta)(1+\beta)]^{1/2}}\gamma_2$
$\mathrm{Im}[a_1^{(2)}(\parallel, \perp)]$	$\frac{-5}{V_2}\frac{\mathrm{Im}[f_2(1,0)]}{[2f_0(1,1)+f_0(0,0)]^{1/2}}$	$\frac{-5\sqrt{3}}{2[(2-\beta)(1+\beta)]^{1/2}}\gamma_2'$
$a_2^{(2)}(\perp)$	$\frac{-5}{2V_2}\frac{f_2(1,-1)}{f_0(1,1)}$	$-\frac{5}{\sqrt{6}}\frac{3}{2-\beta}\eta_2$

The calculations were run over a time period of ∼768 fs, which was sufficient for the lowest energy portion of the wavepacket to reach the end of the grid. In order to optimize the time-step, a reduced calculation was performed solely on the $C\,^1\Pi_{1u}$ state at a number of different time-steps. Convergence was found to occur at 0.024 fs, which was the time-step used in the calculation. The analysis line, (R_d), was assumed to be at 15.5 bohr, 5 bohr beyond the distance of any significant variation in the potentials or couplings. To prevent unphysical reflection of the wavepacket from the end of the grid, a cubic imaginary absorbing potential was placed from $R_d = 15.5$ bohr to $R_{end} = 18.5$ bohr, of the form[47]

$$V_{\mathrm{Damp}}(R) = -\mathrm{i}d_a(2x)^3 \times \begin{cases} x = 0, & R < R_d \\ x = (R - R_d)/(R_{end} - R_d), & R_d \leq R \leq R_{end} \end{cases}, \quad (4)$$

where d_a is the damping parameter. The damping parameter was found to be at its optimum at a value of 0.059 E_H, which gives an absorption of the lowest energy parts of the wavepacket greater than 99.99%. The parameters used in the final calculations are summarized in Table VI. In the following, all the results are for the $^{35}Cl + {}^{35}Cl$ isotopic combination, unless otherwise stated.

III. RESULTS

The dynamical calculations described above produce a complete set of T-matrix elements, including both the magnitude and relative phase. They therefore constitute all of the dynamical information it is possible to obtain for this system.

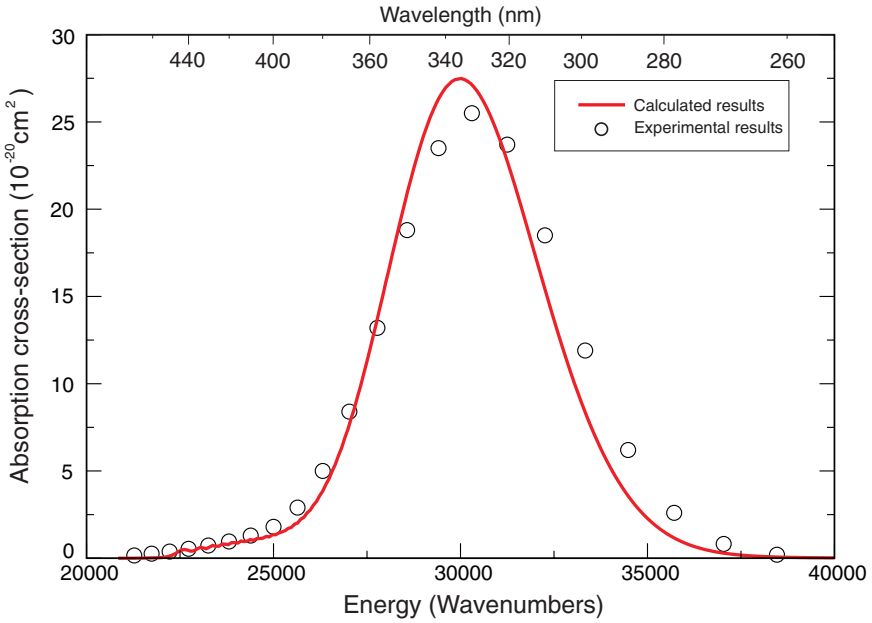

FIG. 6. Simulated values for the total absorption cross-section. Experimental data points from the NIST database[53] provided for comparison.

These quantities, in the form of the partial cross-sections and phase differences, are presented in Sec. III A. Experimentally, the equivalent information is obtained by the angular momentum polarization parameters, which can be calculated from the T-matrix elements.[46] Except for a few cases, the accompanying paper is reserved for a detailed comparison of the present theoretical results with new and existing experimental data on the photodissociation of Cl_2. We employ either the molecular frame polarization parameters of Rakitzis and Zare and co-workers,[8,48] or the laboratory frame polarization parameters of Vasyutinskii and co-workers,[49–51] and the expressions linking these two most commonly employed formalisms are given in Table VII.[46]

Two types of calculated results are presented below, one in which the full potential energy surfaces (including non-adiabatic effects) are used in the calculation, and one in which only the adiabatic potentials shown in Fig. 3 are used, effectively switching off the non-adiabatic interactions. This serves two purposes. Firstly, it allows a check of the dynamics calculations: photodissociation from a single state should have limiting values for the incoherent polarization parameters, and zero values for their coherent counterparts. Secondly, it gives a direct measure of how significant non-adiabatic interactions are in this system.

A. Absorption cross-sections

1. Total absorption cross-section

The total absorption cross-section was calculated using the method of Heller.[52] The unscaled results, along with the IUPAC recommended values,[53] are presented in Fig. 6. The results show a nearly quantitative agreement between the calculations and the experimental data. Generating the total absorption cross-section given by summing the partial cross-sections shown in Fig. 7 gives visually identical results to those presented in Fig. 6.

2. Partial cross-sections and phases

The partial cross-sections are calculated from the square of the T-matrix elements, and as such they represent the probability of the dissociated fragment being in a specific adiabatic state (as opposed to a specific atomic state). They are shown in Fig. 7. The partial cross-sections consist of four states with significant population from the photodissociation process, with the $C\,^1\Pi_{1u}$ state making up the majority of the product flux, with a smaller contribution from the $A\,^3\Pi_{1u}$ state at shorter wavelength, and the $B\,^3\Pi_{0^+u}$ state becoming significant at longer wavelengths. Amongst the states with low partial cross-sections (shown in the lower panel of Fig. 7) there are contributions from two further $\Omega = 1$ states at higher energies: the $(1)^3\Sigma^+_{1u}$ and $(1)^3\Delta_{1u}$ states. In addition, there is also some slight oscillatory fine structure visible for the $B\,^3\Pi_{0^+u}$ state. These oscillations have not been observed experimentally, and may arise from residual noise in the calculations, which is expected near the dissociation threshold.[54] Alternatively they may be real, arising from coupling between the bound levels of the $B\,^3\Pi_{0^+u}$ state and continuum scattering states. Comparison with the partial cross-sections from strictly adiabatic photodissociation shows that both the $A\,^3\Pi_{1u}$ and the $(1)^3\Sigma^+_{1u}$ states are populated from radial non-adiabatic coupling to the $C\,^1\Pi_{1u}$ state, following the mechanism predicted on the basis of the experimental results.[11,12,28]

The cosines of the phase differences between the T-matrix elements of different exit channels, Φ_{mn}, are shown in Fig. 8. They are related to the T-matrix elements by the

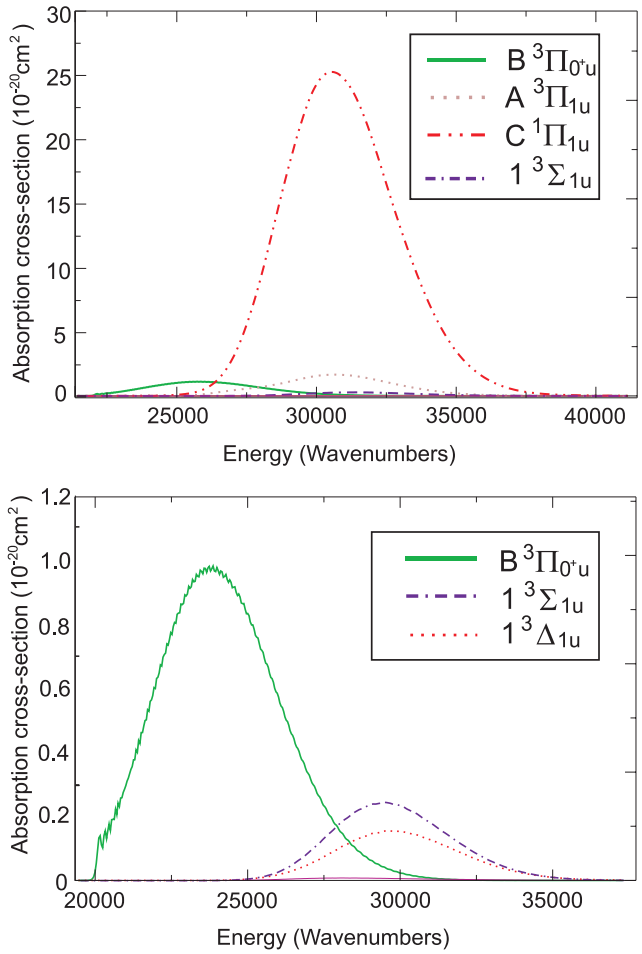

FIG. 7. Upper panel: Partial cross-sections for the full photodissociation calculation. Lower panel: Close-up of states correlating to the (Cl + Cl*) exit channel.

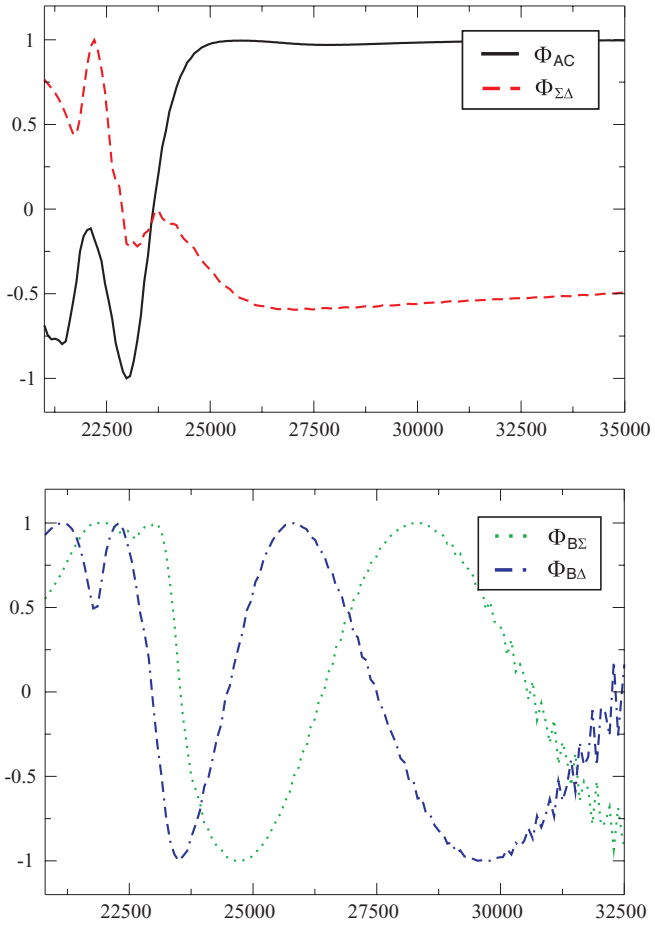

FIG. 8. Graphs showing $\Phi_{mn} = \cos[\phi_m - \phi_n]$, where ϕ_m and ϕ_n are the fragment channels m and n, as a function of photon energy. The top panel corresponds to phase differences between $\Omega = 1$ states, and the bottom panel corresponds to interferences between $\Omega = 1$ and $\Omega = 0$ states. See text for details.

relationship

$$\Phi_{mn} = \cos[\phi_m - \phi_n] = \frac{(\mathrm{Re}[T_m]\mathrm{Re}[T_n] + \mathrm{Im}[T_m]\mathrm{Im}[T_n])}{|T_m||T_n|}. \quad (5)$$

These quantities correspond to interference between fragment channels, and give rise to coherent polarization parameters in the photofragments. Their determination is necessary for the criteria of a complete experiment to be fulfilled.[54] Cases where $\Phi_{mn} > 0$ correspond to constructive interference between fragment channels, whereas $\Phi_{mn} < 0$ corresponds to instances where the channels interfere destructively.

The phase difference between different $\Omega = 1$ states varies slowly over most of the absorption spectrum, with the C $^1\Pi_{1u}$ and A $^3\Pi_{1u}$ states (represented by the parameter Φ_{AC}) interfering constructively, and the $(1)^3\Sigma^+_{1u}$ and $(1)^3\Delta_{1u}$ states (represented by the parameter $\Phi_{\Sigma\Delta}$), both correlating to the (Cl + Cl*) channel, interfering destructively. In contrast, the B $^3\Pi_{0^+u}$ state, also correlating to the (Cl + Cl*) channel, has phase differences with both the $(1)^3\Sigma^+_{1u}$ and $(1)^3\Delta_{1u}$ states (represented by the $\Phi_{B\Sigma}$ and $\Phi_{B\Delta}$ parameters, respectively), which are highly oscillatory with the energy of the dissociating photon. This gives rise to an oscillating $\mathrm{Im}[a_1^{(1)}(\parallel, \perp)]$ polarization parameter for the Cl* fragment from this channel, as discussed in Sec. III D 2.

B. Evolution of the Ω = 1 wavepackets

The wavepacket propagated in these dynamical calculations is a purely theoretical construction,[54] and contains contributions from a large range of energies. Its motion in time does not represent the 'true' time dependence of the dissociation at a well defined energy. Important dynamical information can still be gleaned from studying its evolution in time, however, such as the nature of the non-adiabatic flux between the different potential energy surfaces. In the case of molecular chlorine photodissociation, this is particularly relevant for wavepackets propagating on the adiabatic $\Omega = 1$ surfaces, as the partial cross-sections indicate that there is considerable non-adiabatic flux between the different surfaces at large values of the internuclear coordinate, R. Fig. 9 shows the progress of the wavepackets with time for the four coupled $\Omega = 1$ potentials, A $^3\Pi_{1u}$, C $^1\Pi_{1u}$, $(1)^3\Sigma^+_{1u}$, and $(1)^3\Delta_{1u}$.

Inspection of the evolution of the different wavepackets reveals that

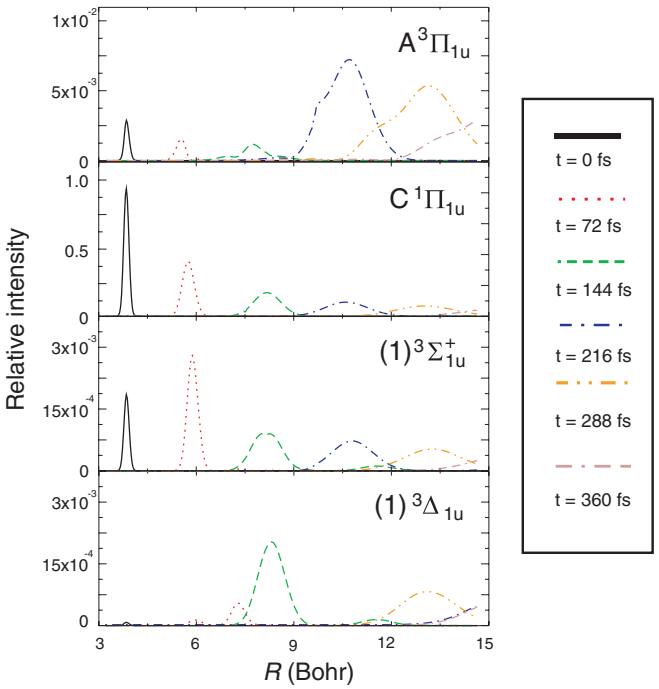

FIG. 9. Wavepackets for the $\Omega = 1$ adiabatic potentials, sampled at different points in time. The *y*-axis scales are normalized to the initial wavepacket in the C $^1\Pi_{1u}$ state.

- The A $^3\Pi_{1u}$ state is mainly populated in the long range region of the potential, at an interatomic distance of between 8 and 10 bohr.
- At $t = 144$ fs the wavepackets of both the $(1)^3\Sigma^+_{1u}$ and $(1)^3\Delta_{1u}$ states display considerable structure, possessing several different maxima. The extremely short lifetime of the excited states, coupled with inspection of Fig. 3 shows that these potentials are repulsive in nature, and hence this bifurcation could not arise as a result of a shape resonance. This feature can therefore be assigned to flux from several coupled surfaces simultaneously.

C. Branching ratio and spatial anisotropy parameters

The top panel of Fig. 10 shows the calculated branching ratio of ground state and excited chlorine atoms over a series of dissociation wavelengths. The low value of the Cl*/Cl branching ratio at short wavelengths shows that the non-adiabatic coupling between the lower lying (C $^1\Pi_{1u}$ and A $^3\Pi_{1u}$) and more excited ($(1)^3\Sigma^+_{1u}$ and $(1)^3\Delta_{1u}$) states is fairly weak at energies in the vicinity of the main absorption maximum, as is confirmed by the partial cross-sections in Fig. 7, and the magnitudes of the different wavepackets in Fig. 9. The spatial anisotropy parameter produced by the calculation for the ground state channel was −1 at every wavelength, as expected for a purely perpendicular excitation. $\beta(E)$ for the excited state channel displays considerably more structure, going from negative values (indicating a perpendicular transition) at short wavelengths to positive values (indicating a parallel transition) at long wavelengths. The results are shown in the bottom panel of Fig. 10. The branching ratio and

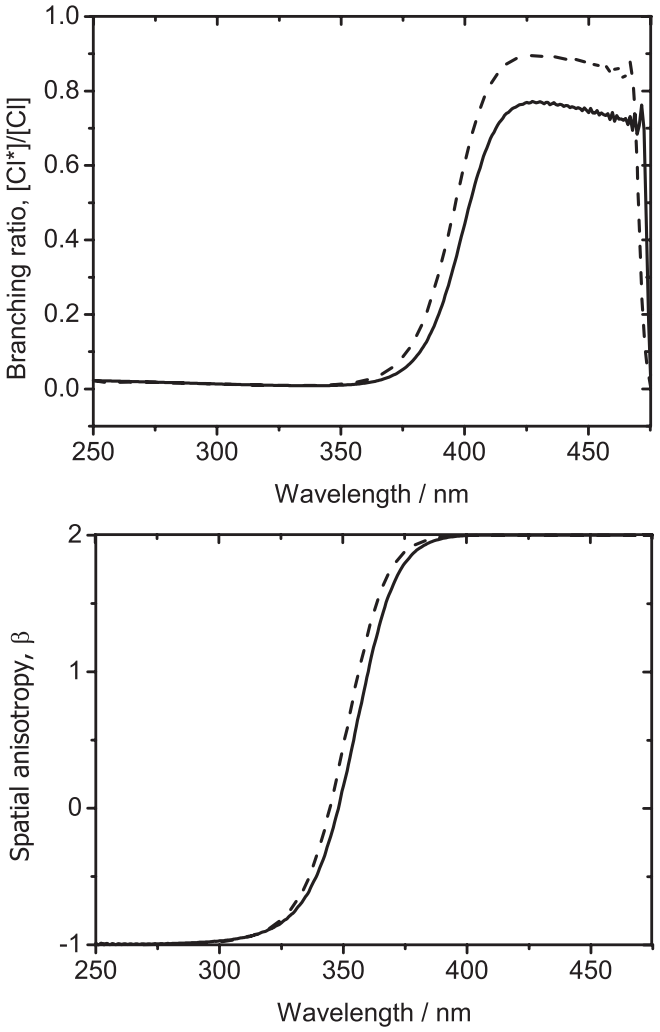

FIG. 10. Top panel: Branching ratio between ground and excited state Cl as a function of wavelength. Bottom panel: Calculated energy dependence of the $\beta(E)$ parameter for fragments in the excited channel. The dashed lines in each panel were obtained using the *R*-dependent transition dipole moments, the continuous lines were with a constant transition dipole moments.[32]

translational anisotropy data are compared with recent experimental results in the accompanying paper.[16] At longer wavelengths, in the low energy tail of the absorption profile, the value of the branching ratio increases markedly.

The data shown as continuous and dashed lines in Fig. 10 were obtained using constant transition dipole moments and with *R*-dependent transition dipole moments, respectively. While there are some differences in the branching ratios obtained for the two levels of calculation, the β parameters are very similar. The polarization parameters to be presented in the following subsection are also very similar for the two types of transition dipole, with the most differences at the extreme long wavelength tail of the absorption spectrum at wavelengths >400 nm.

D. Angular momentum polarization parameters

1. Ground state (Cl + Cl) polarization parameters

The majority of the experimental polarization data available in the literature concerns the low order $K = 1$ and

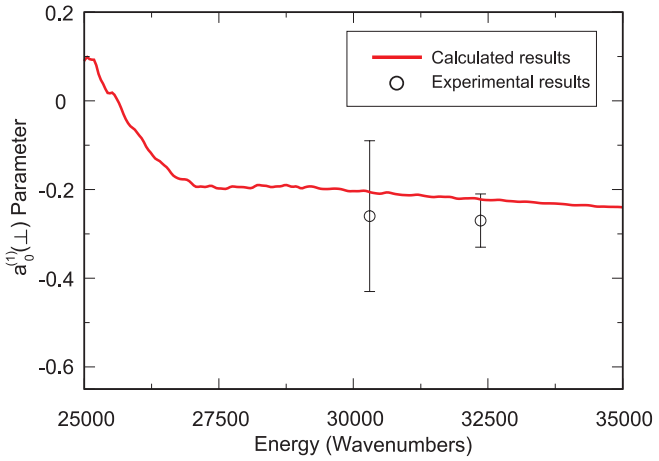

FIG. 11. Energy dependence of the $a_0^{(1)}(\perp)$ polarization parameter of the Cl* fragment, for photodissociation to the (Cl + Cl*) channel. Experimental results, including error bars, from Ref. 8 are provided for comparison.

$K = 2$ orientation and alignment moments for the ground state products of the (Cl + Cl) channel. We defer detailed comparison with experimental data to the accompanying paper,[16] suffice it to say that the agreement between the calculations and the available experimental results is generally very good. The calculations slightly underestimate the incoherent $a_0^{(2)}(\perp)$ parameter, and overestimate the coherent parameter $a_2^{(2)}(\perp)$, suggesting that the calculation might slightly underestimate the non-adiabatic effects in the dissociation.

2. Low order orientation of excited fragments of the (Cl* + Cl) channel

Both of the fragments in the (Cl + Cl*) channel can exhibit angular momentum polarization. The Cl* fragment has been the more extensively investigated of the two: wavelength dependent studies have been performed to determine two polarization parameters, the $a_0^{(1)}(\perp)$ parameter,[8] corresponding to incoherent orientation from a perpendicular state, and $\mathrm{Im}[a_1^{(1)}(\parallel, \perp)]$,[9] corresponding to interference between parallel and perpendicular contributions to the dissociation. The results for the incoherent orientation are shown in Fig. 11, while the results for the coherent orientation, which are compared with both the experimental results from Kim *et al.*[9] and the semi-classical calculations, based on the double slit model, of Asano and Yabushita,[14] are shown in Fig. 12. Note that for $\mathrm{Im}[a_1^{(1)}(\parallel, \perp)]$, we find that the sign of the parameter is inverted compared with the experimental results, for reasons that remain unclear.

The oscillating value of the $\mathrm{Im}[a_1^{(1)}(\parallel, \perp)]$ parameter indicates differing contributions to the Cl* fragment distribution from parallel and perpendicular channels at different dissociation energies. The lower panel of Fig. 7 implies that this is due to interference between the $B\,^3\Pi_{0^+u}$ and the $(1)^3\Sigma_{1u}^+$ and $(1)^3\Delta_{1u}$ channels, with the parallel $B\,^3\Pi_{0^+u}$ channel becoming dominant at lower energies. The quantum dynamical results presented in Fig. 12 show a similar behaviour to the experimental measurements and the semi-classical data, but disagree in magnitude and sign.

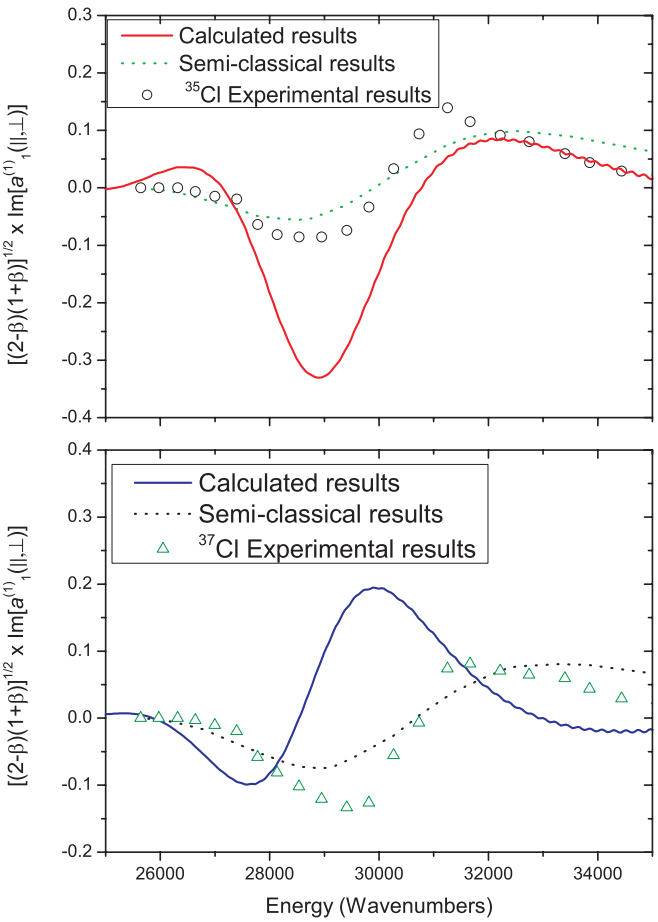

FIG. 12. Top panel: Energy dependence of the $\mathrm{Im}[a_1^{(1)}(\parallel, \perp)]$ polarization parameter for the $^{35}\mathrm{Cl}(^2P_{1/2})$ photofragments as obtained from the full QM dynamical calculations (red continuous line). Experimental results from Kim *et al.*[9] (open circles) are shown for comparison, along with the semi-classical results of Asano and Yabushita (green dotted line).[14] Bottom panel: as for the top panel but showing the QM dynamical results for the $^{37}\mathrm{Cl}(^2P_{1/2})$ photofragments (continuous blue line). The fully quantum dynamics results from this work are compared with the semi-classical results of Asano and Yabushita (black dotted line).[14,16] The experimental results (open green triangles) are taken from Alexander *et al.*[8] Note that in both panels the sign of the theoretical data have been inverted.

The negative, although non-limiting, value of the $a_0^{(1)}(\perp)$ implies that the perpendicular contribution to the (Cl + Cl*) channel is mostly *via* the $(1)^3\Sigma_{1u}^+$ state, as opposed to $(1)^3\Delta_{1u}$ channel. This is again borne out by the partial cross-sections, in which the contribution of the $(1)^3\Delta_{1u}$ channel is found to be small, but non-zero.

3. The effect of isotopic substitution

Experimental investigations have shown a distinct difference in polarization between photofragments of the ^{35}Cl and ^{37}Cl isotopes. In light of the relatively small difference (~6%) in the reduced mass of the two most common chlorine isotopologues, $^{35}\mathrm{Cl}_2$ and $^{35}\mathrm{Cl}^{37}\mathrm{Cl}$, and the apparent validity of the axial recoil approximation in Cl_2 photodissociation (making nuclear spin effects unlikely to be important in the dissociation process), these results are somewhat unexpected. To see if they could be reproduced theoretically, a set of

calculations were performed using the appropriate reduced mass for $^{35}Cl^{37}Cl$. Note that the partial cross-sections generated by the two isotopomers yielded sets of results that can be seen to be extremely close to one another.

The most significant experimental difference between the two isotopomers was seen in the oscillating $\mathrm{Im}[a_1^{(1)}(\parallel, \perp)]$ parameters, where both the magnitude and phase of the parameter could be seen to differ with isotopic substitution. The bottom panel of Fig. 12 compares the experimental and calculated values of $\mathrm{Im}[a_1^{(1)}(\parallel, \perp)]$ for the ^{37}Cl fragment. In spite of the negligible difference in the calculated partial cross-sections, it can be seen that the isotopic substitution does indeed have a significant effect upon this polarization parameter, with the same shift in phase that is observed experimentally. A comparison with the results of the semi-classical double slit model, employed by Asano and Yabushita,[14] is shown in the bottom panel of Fig. 12. As with the data for the ^{35}Cl fragment, the oscillatory behavior is similar in both, but their signs and magnitudes are different.

4. Alignment of ground state Cl in the excited (Cl + Cl*) channel

An interesting, but largely unstudied aspect of this system is the Cl atom from the (Cl + Cl*) channel. This is capable of possessing polarization moments up to $K = 3$, but is paired with an atom which can only possess low order $K = 1$ orientation. The top panel of Fig. 13 shows the coherent $\mathrm{Re}[a_1^{(2)}(\parallel, \perp)]$ alignment parameter for fragment from the (Cl + Cl*) channel, and shows that the alignment, as well as the orientation, could be expected to be non-zero and highly oscillatory with photon energy. The dynamical calculations indicate that three different states are involved in the photodissociation to the excited channel, meaning that five different quantities (three magnitudes and two phase differences) are required to fully characterize the dynamics of this channel, and the determination of the excited state alignment would be a necessary part of this. These higher order polarization moments are determined for the first time in the accompanying paper.[16]

5. High order orientation in the (Cl + Cl) channel

The bottom panel of Fig. 13 shows the calculated higher order orientation moments for the (Cl + Cl) channel. The coherent $a_2^{(3)}(\perp)$ parameter is small but non-zero, as would be expected for the coupled A and C states. More significant is the large negative value for the incoherent $a_0^{(3)}(\perp)$ parameter. This is large enough to be significant in experimental signals. Again, as with the data in the previous subsection, this aspect of the angular momentum polarization is explored more fully in the accompanying paper.[16]

6. Adiabatic results

The results presented here are generated from a calculation on the adiabatic potential energy curves shown in Fig. 3, but with the adiabatic-diabatic transformation matrix

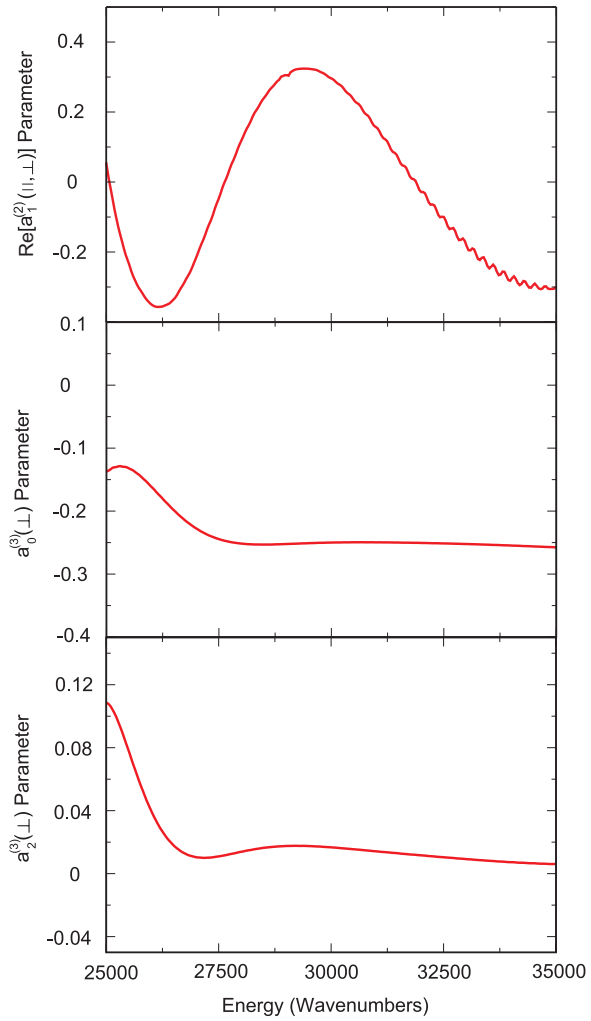

FIG. 13. Top panel: Coherent $\mathrm{Re}[a_1^{(2)}(\parallel, \perp)]$ polarization parameter for the Cl fragment in the (Cl + Cl*) channel. Middle and bottom panels: Orientation polarization parameters for the Cl atoms produced in the ground (Cl + Cl) channel.

set as the unit operator,

$$c_{jk,u}(R) = \delta_{jk}\,. \tag{6}$$

This will therefore give the results as they would be in the case where non-adiabatic effects were negligible. The resulting partial cross-sections are identical to the molar extinction coefficients given in Figure 5 of the original electronic structure calculations paper by Kokh *et al.*[32]

Within this approximation, the only two significantly populated states are the $B^3\Pi_{0^+u}$ and $C\,^1\Pi_{1u}$ states, as these are the states populated in the excitation step. The $B^3\Pi_{0^+u}$ state is populated in spite of the adiabatic approximation because the initial state has a small triplet component. Incoherent contributions from these two states would therefore be expected to dominate the polarization parameters of the (Cl + Cl*) and (Cl + Cl) channels, respectively. Tables VIII and IX show the results of the adiabatic calculations, together with both the experimental results and the results of the full dynamics calculation, at several points over the photodissociation spectrum. While the adiabatic results provide a rationale for some of the incoherent polarization parameters, the full calculation is

TABLE VIII. Table of polarization parameters for photodissociation to the (Cl + Cl) channel. Columns from left to right: polarization parameter being determined, wavelength of the experiment performed, results from experiment,[8,12,26,28] results from the adiabatic calculation, results from the full calculation, limiting values of the polarization moment.

Parameter	Wavelength (nm)	Experimental result	Adiabatic calculation	Full calculation	Limiting values
$a_0^{(2)}(\perp)$	308	−0.62(9)	−0.8	−0.70	±0.80
	320	−0.50(10)	−0.8	−0.70	
$a_2^{(2)}(\perp)$	308	−0.26(7)	0.0	−0.27	±0.490
	320	−0.32(6)	0.0	−0.26	
	355	−0.30(10)	0.02	−0.26	
$a_0^{(1)}(\perp)$	310	0.13(2)	0.26	0.26	±0.775
	330	0.23(1)	0.26	0.26	

required to capture the complete set of coherent and incoherent parameters and their wavelength dependencies.

7. Effect of molecular rotation

As we have noted in Sec. I, the present theoretical treatment neglects the effect of parent rotational angular momentum. Schemes for approximately treating these effects have recently become available,[55] and, in the absence of significant Coriolis interactions, demonstrate that parent molecule rotation can be treated as a well defined reduction factor from those which would be obtained if the axial recoil approximation was valid. Vasyutinskii and co-workers[55–57] have shown that these reduction factors take the form of reduced rotation matrix elements with a 'classical rotation' angle γ. If it is assumed that photodissociation to the (Cl + Cl) exit channel is entirely perpendicular in character, and so should give an axial recoil value of $\beta(E) = -1$, it is possible to estimate the value of γ from the reduction of the experimentally obtained $\beta(E)$ from this limiting value. This can then be used to work out approximate 'correction factors' for the calculated or experimentally measured alignment moments. Hence it is possible to obtain a qualitative insight into the effects of axial recoil.

The theoretical treatment of Vasyutinskii and co-workers[55] was developed using the space frame anisotropy parameters, as opposed to the body frame polarization parameters used in this paper. Expressions to convert between the two sets were given in the review by Suits and Vasyutisnkii[46]

TABLE IX. Table of polarization parameters for photodissociation to the (Cl + Cl*) channel, for the Cl* atoms. Experimental results of Alexander *et al.*,[8] results of the adiabatic calculation, results of the full calculation, and the theoretical limiting values of the polarization moments are provided for comparison. Note that the for $\mathrm{Im}[a_1^{(1)}(\parallel, \perp)]$ the sign of the results from the full calculation have been reversed.

Parameter	Wavelength (nm)	Experimental result	Adiabatic calculation	Full calculation	Limiting values
$a_0^{(1)}(\perp)$	310	−0.24(1)	0.00	−0.20	±0.577
	330	−0.26(17)	0.00	−0.20	
$\mathrm{Im}[a_1^{(1)}(\parallel, \perp)]$	310	0.10(1)	0.26	0.10	±0.408
	330	0.032(5)	0.26	−0.10	

TABLE X. Table of appropriate correction factors to convert the experimental polarization moments to their axial recoil values (their limiting values in the absence of parent molecule rotation). Note that the γ values are estimate on the basis of the observed deviations in β from the limiting value of −1. The s_2 factor has not been included because it is unaffected by parent molecule rotation, and so its correction factor in all instances would be 1.

Wavelength (nm)	Rotation angle (radians)	Parameter	Correction factor
308	$\gamma = 0.29$	$\beta(E)$	1.14
		α_2	1.14
		η_2	1.04
320	$\gamma = 0.20$	$\beta(E)$	1.07
		α_2	1.07
		η_2	1.02
355	$\gamma = 0.20$	$\beta(E)$	1.07
		α_2	1.07
		η_2	1.02

and are also provided in the accompanying paper. In this instance the necessary parameters (α_2, s_2, and η_2) were calculated in the time-of-flight frame, the appropriate correction factors applied, and then used to generate the new $a_q^{(k)}(p)$ moments. The correction factors employed in the space fixed frame are shown in Table X. Although the correction factors are quite close to unity, and the effects of non-axial recoil therefore relatively small, the inclusion of this rotational smearing tends to bring the experimental and simulated data into slightly better agreement, although discrepancies with $a_0^{(2)}(\perp)$ at longer wavelengths remain significant.

IV. SUMMARY AND CONCLUSION

A fully quantum mechanical, time dependent computation has been used to simulate the photodissociation of Cl_2 in its first absorption band. This constitutes the first complete study of the dissociation for a molecule of this complexity. A complete set of polarization parameters have been obtained for photodissociation over a range of energies. Where experimental results are available, agreement between them and the calculations is very good, barring a mild discrepancy in the magnitude of the non-adiabatic coupling between the $C\,^1\Pi_{1u}$ and $A\,^3\Pi_{1u}$ states.

The calculations confirm the currently accepted mechanism for the dissociation, that it occurs primarily from excitation to the $C\,^1\Pi_{1u}$ state, with significant non-adiabatic coupling to the $A\,^3\Pi_{1u}$ state, and a weaker transition to the $(1)^3\Sigma_{1u}^+$ state, which correlates to the excited (Cl + Cl*) channel. This channel is further populated at longer wavelengths by excitation to the $B\,^3\Pi_{0^+u}$ state, and, where this pathway occurs at the same wavelength as that *via* the $(1)^3\Sigma_{1u}^+$ state, there is significant quantum mechanical interference between the two.

Although experimental results have been obtained at several different places in the absorption spectrum, they have been performed over a period of several years, and using several different methods. In order to obtain a consistent set of data, and also to determine the higher order parameters which these results indicate might be significant, it would be

interesting to repeat the experiments over a series of different photolysis wavelengths, using a sufficient number of geometries to extract all of the polarization parameters. The results of such a study is presented in the accompanying paper.[16]

ACKNOWLEDGMENTS

This work was supported by the U.K. EPSRC (to M.B. *via* Programme Grant No. EP/G00224X1), the E.U. (to M.B. *via* FP7 EU People ITN project 238671) and the Deutsche Forschungsgemeinschaft (to R.J.B. *via* Grant No. BU 450/21-2). Valuable discussions with Dr G.A.D. Ritchie are gratefully acknowledged. A.B. thanks the Natural Sciences Engineering Research Council of Canada (Discovery Grant) for financial support.

[1] M. J. Molina, T. Tso, L. T. Molina, and F. C. Wang, Science **238**, 1253 (1987).
[2] L. G. M. de Macedo and W. A. de Jong, J. Chem. Phys. **128**, 041101 (2008).
[3] R. W. Diesen, J. C. Wahr, and S. E. Adler, J. Chem. Phys. **50**, 5635 (1969).
[4] G. E. Busch, R. T. Mahoney, R. I. Morse, and K. R. Wilson, J. Chem. Phys. **51**, 449 (1969).
[5] A. S. Bracker, E. R. Wouters, A. G. Suits, and O. S. Vasyutinskii, J. Chem. Phys. **110**, 6749 (1999).
[6] L. Li, R. J. Lipert, J. Lobue, W. A. Chupka, and S. D. Colson, Chem. Phys. Lett. **151**, 335 (1988).
[7] Y. Matsumi, M. Kawasaki, T. Sato, T. Kinugawa, and T. Arikawa, Chem. Phys. Lett. **155**, 486 (1989).
[8] A. J. Alexander, Z. H. Kim, S. A. Kandel, R. N. Zare, T. P. Rakitzis, Y. Asano, and S. Yabushita, J. Chem. Phys. **113**, 9022 (2000).
[9] Z. H. Kim, A. J. Alexander, S. A. Kandel, T. P. Rakitzis, and R. N. Zare, Faraday Discuss. **113**, 27 (1999).
[10] L. D. A. Siebbeles, M. Glass-Maujean, O. S. Vasyutinskii, J. A. Beswick, and O. Roncero, J. Chem. Phys. **100**, 71913610 (1994).
[11] T. P. Rakitzis, P. C. Samartzis, R. L. Toomes, T. N. Kitsopoulos, A. Brown, G. G. Balint-Kurti, O. S. Vasyutinskii, and J. A. Beswick, Science **300**, 1936 (2003).
[12] M. J. Bass, M. Brouard, A. P. Clark, B. Martínez-Haya, and C. Vallance, Phys. Chem. Chem. Phys. **5**, 856 (2003).
[13] A. P. Clark, M. Brouard, F. Quadrini, and C. Vallance, Phys. Chem. Chem. Phys. **8**, 5591 (2006).
[14] Y. Asano and S. Yabushita, J. Phys. Chem. A **105**, 9873 (2001).
[15] Y. Asano and S. Yabushita, Chem. Phys. Lett. **372**, 348 (2003).
[16] E. K. Campbell, A. B. Alekseyev, G. G. Balint-Kurti, M. Brouard, A. Brown, R. J. Buenker, R. Cireasa, A. Gilchrist, A. J. Johnsen, D. B. Kokh, S. Lucas, G. A. D. Ritchie, T. R. Sharples, and B. Winter, J. Chem. Phys. **136**, 164311 (2012).
[17] R. S. Mulliken, Phys. Rev. **36**, 1440 (1930).
[18] Y. Matsumi, K. Tonokura, and M. Kawasaki, J. Chem. Phys. **97**, 1065 (1992).
[19] A. S. Bracker, "An investigation of polarized atomic photofragments using the ion imaging technique," Ph.D. dissertation (University of California, Berkeley, 1997).
[20] J. A. Wheeler and W. H. Zurek, *Quantum Theory and Measurement*, 1st ed. (Princeton University Press, 1984).
[21] P. C. Samartzis, I. Sakellariou, T. Gougousi, and T. N. Kitsopoulos, J. Chem. Phys. **107**, 43 (1997).
[22] Y. Wang, H.-P. Loock, J. Cao, and C. X. W. Qian, J. Chem. Phys. **102**, 808 (1995).
[23] Y. B. Band, K. F. Freed, and D. J. Kouri, Chem. Phys. Lett. **79**, 233 (1981).
[24] Y. B. Band, K. F. Freed, and S. J. Singer, J. Chem. Phys. **84**, 3762 (1986).
[25] A. S. Bracker, E. R. Wouters, A. G. Suits, Y. T. Lee, and O. S. Vasyutinskii, Phys. Rev. Lett. **80**, 1626 (1998).
[26] T. P. Rakitzis, S. A. Kandel, A. J. Alexander, Z. H. Kim, and R. N. Zare, J. Chem. Phys. **110**, 3351 (1999).
[27] P. C. Samartzis, B. L. G. Bakker, T. P. Rakitzis, D. H. Parker, and T. N. Kitsopoulos, J. Chem. Phys. **110**, 5201 (1999).
[28] T. P. Rakitzis and T. N. Kitsopoulos, J. Chem. Phys. **116**, 9228 (2002).
[29] S. D. Peyerimhoff and R. J. Buenker, Chem. Phys. **57**, 279 (1981).
[30] C. Jönsson, Am. J. Phys. **42**, 4 (1974).
[31] D. B. Kokh, A. B. Alekseyev, and R. J. Buenker, J. Chem. Phys. **115**, 9298 (2001).
[32] D. B. Kokh, A. B. Alekseyev, and R. J. Buenker, J. Chem. Phys. **120**, 11549 (2004).
[33] G. G. Balint-Kurti, A. J. Orr-Ewing, J. A. Beswick, A. Brown, and O. S. Vasyutinskii, J. Chem. Phys. **116**, 10760 (2002).
[34] A. Brown, G. G. Balint-Kurti, and O. S. Vasyutinskii, J. Phys. Chem. A **108**, 7790 (2004).
[35] A. G. Smolin, O. S. Vasyutinskii, G. G. Balint-Kurti, and A. Brown, J. Phys. Chem. A **110**, 5371 (2006).
[36] R. J. Buenker and S. D. Peyerimhoff, Theor. Chim. Acta **35**, 33 (1974).
[37] S. Krebs and R. J. Buenker, J. Chem. Phys. **103**, 5613 (1995).
[38] L. R. Kahn, P. Baybutt, and D. G. Truhlar, J. Chem. Phys. **65**, 3826 (1976).
[39] A. B. Alekseyev, H.-P. Liebermann, and R. J. Buenker, in *Relativistic Molecular Calculations*, edited by K. Hirao and M. Ishikawa (World Scientific, Singapore, 2003), pp. 65–105.
[40] R. J. Buenker and S. D. Peyerimhoff, Theor. Chim. Acta **12**, 183 (1968).
[41] P. Huxley and J. N. Murrell, J. Chem. Soc. Faraday Trans II. **79**, 323 (1983).
[42] C. C. Marston and G. G. Balint-Kurti, J. Chem. Phys. **91**, 3571 (1989).
[43] M. D. Feit and J. A. Fleck, J. Chem. Phys. **78**, 301 (1983).
[44] D. Kosloff and R. Kosloff, J. Comput. Phys. **52**, 35 (1983).
[45] G. G. Balint-Kurti, R. N. Dixon, and C. C. Marston, J. Chem. Soc. Faraday Trans. **86**, 1741 (1990).
[46] A. G. Suits and O. S. Vasyutinskii, Chem. Rev. **108**, 3706 (2008).
[47] A. Vibok and G. G. Balint-Kurti, J. Phys. Chem. **96**, 8712 (1992).
[48] T. P. Rakitzis and R. N. Zare, J. Chem. Phys. **110**, 3341 (1999).
[49] O. S. Vasyutinskii, Sov. Phys. JETP **54**, 855 (1981).
[50] O. S. Vasyutinskii, Opt. Spectrosc. **54**, 524 (1983).
[51] B. V. Picheyev, A. G. Smolin, and O. S. Vasyutinskii, J. Phys. Chem. A **101**, 7614 (1997).
[52] E. J. Heller, J. Chem. Phys. **68**, 2066 (1978).
[53] See http://www.iupac-kinetic.ch.cam.ac.uk/ for "IUPAC Subcommittee on Gas Kinetic Data Evaluation."
[54] G. G. Balint-Kurti, A. Brown, and O. S. Vasyutinskii, Physica Scipta. **73**, C76 (2006).
[55] V. V. Kuznetsov and O. S. Vasyutinskii, J. Chem. Phys. **123**, 034307 (2005).
[56] P. S. Shternin and O. S. Vasyutinskii, J. Chem. Phys. **128**, 194314 (2008).
[57] V. V. Kuznetsov, P. S. Shternin, and O. S. Vasyutinskii, J. Chem. Phys. **13**, 134312 (2009).
[58] A. G. Smolin, O. S. Vasyutinskii, E. R. Wouters, and A. G. Suits, J. Chem. Phys. **121**, 6759 (2004).